Journal of Molecular Structure 1134 (2017) 226–236

Contents lists available at ScienceDirect

Journal of Molecular Structure

journal homepage: http://www.elsevier.com/locate/molstruc

Structural and spectral analysis of 3-metoxytyramine, an important metabolite of dopamine

Dušan Dimić [a], Dejan Milenković [b], Zoran Marković [c], Jasmina Dimitrić Marković [a, *]

[a] Faculty of Physical Chemistry, University of Belgrade, 12-16 Studentski trg, 11000, Belgrade, Serbia
[b] Bioengineering Research and Development Center, Prvoslava Stojanovića 6, 34000, Kragujevac, Serbia
[c] Department of Chemical-Technological Sciences, State University of Novi Pazar, Vuka Karadžića bb, 36300, Novi Pazar, Serbia

ARTICLE INFO

Article history:
Received 26 July 2016
Received in revised form
25 October 2016
Accepted 26 December 2016
Available online 28 December 2016

Keywords:
3-Methoxytyramine
IR
Raman
NMR
B3LYP
QTAIM
NBO

ABSTRACT

Density functional theory calculations, with B3LYP functional and 6-311++G(d,p) basis set are performed with the aim to support the molecular structure and the spectroscopic characteristics of 3-methoxytyramine, the major extracellular metabolite of dopamine. Natural Bond Orbital (NBO) and Quantum Theory of Atoms in Molecules (QTAIM) analysis were used to explain the specific interactions in the most stable conformations in vacuum and water. The conformer resembling the crystallographic structure was compared to the experimentally available data and NMR spectra. The detailed vibrational spectral analysis and the assignments of the bands, done on the best-fit basis comparison of the experimentally obtained and theoretically calculated IR and Raman spectra, match quite well indicating DFT calculations as very accurate source of normal mode assignments. The obtained results demonstrate the applicability and performance of DFT calculations in conformational analysis of 3-methoxytyramine at the state of the isolated molecule. The molecular docking showed that the most stable conformation in vacuum was not the most stable one when docked in protein, proving that only the weak interactions stabilize the gaseous phase conformations.

1. Introduction

Dopamine (DA) is catecholamine which functions as hormone and neurotransmitter in the peripheral endocrine and the central nervous system. Dopamine and its metabolites continue to receive considerable research attention due to their extraordinarily important functions under *in vivo*. It is known that they regulate physiological processes and are considered as the main chemicals in the development of endocrine, cardiovascular, neurological and psychiatric diseases [1,2].

The major extracellular metabolite of dopamine, 3-methoxytyramine (3-MT, aka 3-methoxy-4-hydroxyphenethylamine, 4-(2-aminoethyl)-2-methoxyphenol or 3-*O*-methyldopamine), is produced by dopamine methylation via catechol-*O*-methyltransferase (COMT) [3]. 3-MT is not just an inactive metabolite of dopamine, but a neuromodulator [4] that in certain cases may be involved in movement control. It can be further decomposed to homovanillic acid by monoamine oxidase and aldehyde dehydrogenase. Its complete characterization can be helpful in understanding the pathophysiology of brain disorders which lead to schizophrenia, Parkinson's and some other diseases [1,2]. According to the literature data [5] 3-MT could be a very good indicator for the decreased release of dopamine because the change in release of this neurotransmitter is rapidly reflected in formation of 3-MT. The elevated concentrations of 3-MT, along with other cathecholamines, may indicate mental disorders as well as the development of pheochromoecytomas and paragangliomas (PPGL), tumors arising from the adrenal and extra-adrenal chromaffin cells [6–10]. The laboratory tests have also shown that 3-MT concentration is associated with the tumor size and genetics of PPG [11–13]. However, the experimental data from patients with this type of tumor, have proved that the investigated compound has controversial place. The results were in favor of the non-specificity associated with the dopamine-secreting PPGL and there were no differences in 3-MT concentration between different tumors diagnosed [14]. Due to its importance there are several fast techniques developed for determination of its concentration, including the automated fluorimetric assay [15], the liquid chromatography with the amperometric detection in urine [16,17], and mass fragmentation from rat brain [18].

* Corresponding author.
E-mail address: markovich@ffh.bg.ac.rs (J.D. Marković).

http://dx.doi.org/10.1016/j.molstruc.2016.12.082
0022-2860/

The present study comprises *in vitro* experimental (IR, Raman, NMR, UV–vis, crystallographic) and DFT theoretical approaches in analysis of 3-MT structure which, to the best of our knowledge, have not been done yet. The other metabolites of dopamine, 3,4-dihydroxyphenylacetic acid (DOPAC) [19] and homovanillic [20], were investigated by the means of DFT calculation and compared to the experimental spectra. For the detailed theoretical description of the investigated molecule various methods were used: Natural Bond Orbital (NBO), Quantum Chemistry of Atoms in Molecules (QTAIM), TD-DFT, Potential Energy Distribution (PED) and Gauge Independent Atomic Orbital (GIAO) analysis. Comparison of the obtained spectra and the theoretical calculations has been performed in order to verify the predicted stability of conformers and discuss the specific interactions governing the structure.

2. Experimental and computational methods

2.1. Experimental

2.1.1. Chemicals

3-MT was purchased from a commercial source (Aldrich) and was used without further purification. Potassium bromide (IR grade) was also purchased from a commercial source (Aldrich).

2.1.2. IR, Raman, UV–Vis and NMR spectra

The IR spectrum was recorded on Avatar 370 -Thermo Nicolet FTIR spectrometer. The spectrum was recorded in the middle, 4000–400 cm^{-1}, IR region with the spectral resolution of 2 cm^{-1}. 3 MT was studied in the potassium bromide matrix with a ratio of (1: 200) mg (3 MT: KBr).

The Raman spectrum was registered on a Thermo Scientific DXR Raman microscope in the 3500–400 cm^{-1} range. The spectrum was excited with the diode pumped solid state high-brightness 532 nm laser. The objective lens was 50 × . The scattered light was analyzed by the spectrograph with a 900 lines/mm grating. The spectrum was obtained directly from the pure powder samples. The laser output was kept at 10 mW. Acquisition time was 10 s with 10 scans. The fluorescence correction has been done. Thermo Scientific OMNIC software was used for data acquisition and data processing.

The Raman scattering activities were used for derivation of the theoretical Raman intensities (I_i^R):

$$I_i^R = C(\upsilon_0 - \upsilon_i)^4 \cdot \upsilon_i^{-1} \cdot B_i^{-1} \cdot S_i \quad (1)$$

The quantity B_i is temperature factor including the contribution of excited vibrational states, as predicted by Boltzmann distribution.

$$B_i = 1 - \exp\left(-\frac{h\upsilon_i c}{kT}\right) \quad (2)$$

In Equations (1) and (2) the quantities have the following meanings: h, k, c, and T are Planck and Boltzmann constants, speed of light and temperature, respectively. υ_0 is the wavenumber of the laser excitation line ($\upsilon_0 = 18797$ cm^{-1} corresponding to 532 nm), υ_i is the wavenumber of the normal mode (cm^{-1}), while S_i is the Raman scattering activity of the normal mode Q_i. The calculated Raman intensity,I_i^R, is expressed in arbitrary units (C is a constant equal to 10^{-12}). The value of factor B_i was assumed to be 1 due to low contribution of the excited vibrational states. The calculated Raman intensities for the bands below 300 cm^{-1} were extremely overestimated when compared to the experimental values [21].

The NMR spectra were recorded on a Varian Gemini 200 MHz NMR spectrometer (^1H at 200 and ^{13}C at 50 MHz). The spectra were recorded in DMSO-d_6 with TMS as the internal standard. The UV–Vis spectrum of the water solution of 3-methoxytyramine was obtained on Cintra GB 10 UV–Vis spectrophotometer in the range between 210 and 320 nm.

2.2. Theoretical

All of the calculations presented in this paper were performed in the Gaussian Program Package [22] with B3LYP functional [23] in conjunction with 6–311++G(d,p) [24] basis set. The most stable conformers of the protonated 3-methoxytyramine were determined by the rotation of the aliphatic chain around two dihedral angles and minima of the potential energy surface were identified. The stable conformers were obtained by full optimization and no imaginary frequencies were present. In order to encounter for the possible solvent effects SMD model [25] was used. TD-DFT approach [26] was employed for predicting the electronic transitions and calculation of the parameters important for the theoretical UV-VIS spectra. The vibrational (Infra-red and Raman) spectra were calculated based on the gas-phase geometries. For the analysis of the normal modes VEDA program [27] and PED (Potential Energy Distribution) analysis [28] were performed in order to obtain the percentage of the normal modes in all of the calculated frequencies. GIAO (Gauge Independent Atomic Orbital) approach [29,30] was used for the simulation of NMR spectra of the investigated compound relative to TMS. The Natural Bond orbital (NBO) analysis [31] was performed for the explanation of the interactions inside the molecule and visualization of the orbitals involved in the electronic transitions. The specific intramolecular interactions were further investigated by the means of Quantum Theory of Atoms in Molecules (QTAIM) [32]. The molecular docking simulations were carried out using the AutoDock 4.0 software. The three-dimensional crystal structure of Human C-Reactive Protein was obtained from Protein Data Bank (PDB ID:1b09) [33]. The protein was prepared for docking by removing the co-crystallized ligand, water molecules and co-factors using the Discovery Studio 4.0 [34]. AutoDockTools (ADT) graphical user interface was used to calculate Kollman charges and to add polar hydrogen. In this automated docking program, the flexibility of the ligands was considered while the protein or biomolecules was considered as a rigid structure. All bonds of the ligands were set to be rotatable. All calculations for protein-ligand flexible docking were done using the Lamarckian Genetic Algorithm (LGA) method. The grid box with a dimension of 124.5 × 150.4 × 6.322 points was used so as to cover the protein binding site and accommodate the ligands to move freely. Although the used ligands showed from seven to fifteen possible docking positions, only the best ones are presented. The iInhibition potency of the deprotonated and protonated forms of 3-MT were investigated.

3. Results and discussion

3.1. Geometry optimization

The structure of dopamine and its metabolite, 3-methoxytyramine (3-MT) differ only in methoxy group which replaces hydroxyl group (Fig. 1.). This induces several changes in the possible conformer search because of the volume of this group and the lost ability for the formation of hydrogen bond with other OH group. The starting structures for the geometry optimization are those discussed as crystallographic structures [35]. For the conformer search, there are three positions of hydroxyl and methoxy groups relative to the aliphatic chain: to the left (***l***) (where the hydrogen bond is formed O–H···O–CH_3), to the right (***r***) (no hydrogen bond is formed) and opposite (***o***) (Supplementary

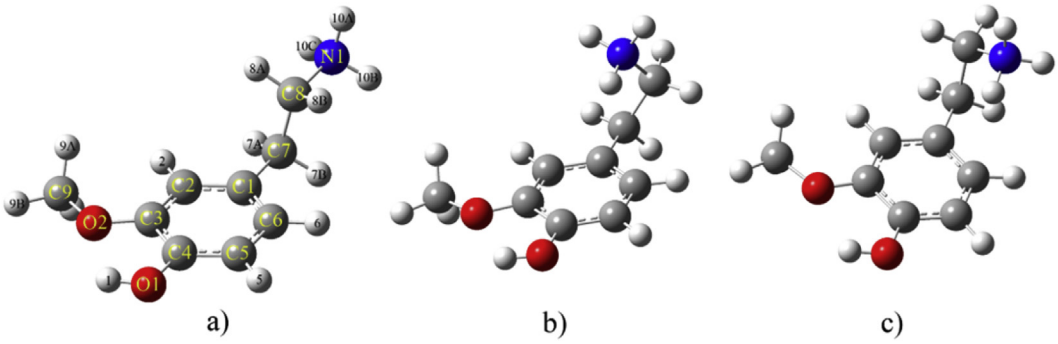

Fig. 1. Structure of the most stable conformers of 3-methoxytyramine in gas phase: a) **1-l** (with atom numbering), b) **3-l** and c) **4-l**.

material, Fig. S1). The rotation in these structures is allowed around two angles, denoted as α(C1–C7–C8–N1) and β(C6–C1–C7–C8). During the geometry optimization twelve stable rotamers, four for each relative position of the side groups, were obtained and their structures are shown in Supplementary material, Fig. S1. Tables S1 and S2 give the differences in enthalpies and Gibbs free energies for all of the investigated conformers in vacuum and for conformers with the left and the opposite orientation in aqueous solutions. Based on the thermodynamic parameters, the most stable conformers are those with the left orientation of the side groups. The general order of conformers is *l* < *o* < *r*, within range 0–54 kJ/mol, proving the importance of the positions of hydroxyl and methyl groups. This agrees with the previous theoretical investigation of the similar molecules [19,20,36]. Three most stable conformers, relevant for the further discussion, are presented in Fig. 1. The corresponding Cartesian coordinates are presented in Supplementary material (Tables S3, S4 and S5).

The most stable conformer of 3-MT resembles the one obtained for dopamine by Lagutschenkov et al. [36], proving that the methoxy group does not have the significant effect on structure. Both of the *gauche* conformations, **3-l** and **4-l**, are more stable than *anti*, **1-l**, by more than 20 kJ/mol. The rotation barriers of 1 → 3 and 1 → 4 transitions for the protonated form are relatively high, around 40 kJ/mol, and 25 kJ/mol for 3 → 4 transition. As discussed in previous works [37], in *gauche* conformation of 2-phenethylamines NH_3^+ can possibly interact with π-system of aromatic ring. Because of this in systems like $X–CH_2–CH_2–NH_3^+$, the *gauche* conformation is more stable if X is aromatic ring, as found in other similar compounds like dopamine [38], histamine [39] and 2-phenethylamines [37]. One the most prominent structural changes between the *anti* and *gauche* conformations is the elongation of one of the N–H bonds in latter as a sign of stabilization and formation of N–H … π interactions. All of the N–H bonds in **1-l** are of the order of 1.024 Å, while in **3-l** and **4-l** structures one of N–H bonds is 1.033 and 1.037 Å respectively which, can be taken as the result of the strong interaction of proton donor with aromatic ring. The global minima in the protonated **3-l** form are characterized by the intramolecular N–H … $C_{aromatic}$ bond lengths of 2.34 Å (with C1) and 2.98 Å (with C2). The global minima in the protonated **4-l** form are 2.35 Å for N–H···C1 and 2.36 Å for N–H···C2. All these bond lengths are observed in stable conformers of dopamine [36].

In the protonated form, the differences in energy in aqueous solutions are much lower, of the order of several kJ/mol, probably because of the interactions between molecule and the polarizable continuum and NH_3^+ and the aromatic ring which are comparable in strength. More detailed analysis of the intramolecular interactions, explaining the stability of these conformations, is given in QTAIM and NBO analysis section of the paper.

3.2. Comparison with crystal structure

The crystal structure of the investigated molecule was determined by Okabe and coworkers [35]. The obtained structure has the amino side chain perpendicular to the catechol ring, which contradicts the structure of the rest of catecholamines [35]. In the previously mentioned reference of Okabe this structure is discussed to resemble the biologically very reactive dopamine conformer. From the theoretical point this structure is a transition state during the rotation around the dihedral angle and cannot be considered as stable, especially with the oppositely directed groups having larger energy differences.

The experimental crystallographic parameters for 3-methoxytyramine hydrochloride are compared to those calculated for the elongated structure, because of the resemblance – **1-l** and results given in Table 1. The numeration of atoms that follows the reference data of Okabe and Mori [40] is given in Fig. 1. The values for bonds are, in all cases, overestimated about 0.02 Å, while the values for the catechol moiety and C–O being very well reproduced. The difference of 0.04 Å, is observed for a single N1–C8 and C7–C8 bond in the aliphatic chain and this can be understood as a consequence of the free rotation around this bond. When it

Table 1
The comparison of experimental and theoretical values of structural parameters.

Bond/angle	Experimental	Theoretical
O1–C4	1.37	1.35
O2–C3	1.38	1.36
O2–C9	1.43	1.43
N2–C8	1.48	1.54
C1–C2	1.39	1.40
C1–C6	1.39	1.39
C1–C7	1.52	1.52
C2–C3	1.38	1.39
C3–C4	1.40	1.41
C4–C5	1.36	1.39
C5–C6	1.40	1.39
C7–C8	1.48	1.53
C3–O2–C9	118.2	119.4
C2–C1–C6	118.2	119.4
C2–C1–C7	119.0	120.2
C6–C1–C7	122.8	120.3
C1–C2–C3	121.4	120.1
O2–C3–C2	125.0	126.2
O2–C3–C4	114.6	113.7
C2–C3–C4	120.3	120.1
O1–C4–C3	116.8	120.5
O1–C4–C5	124.6	119.8
C3–C4–C5	118.6	119.7
C4–C5–C6	121.1	120.1
C1–C6–C5	120.4	120.7
C1–C7–C8	115.1	109.9
N1–C8–C7	113.3	111.0

comes to angles, these values were also reproduced well within 2°, except in certain cases, but with the differences somewhat lager in comparison to those obtained for the bond lengths. In general, the theoretically obtained values have been larger. The largest discrepancy in angle values is obtained for O1–C4–C3 and O1–C4–C5, because of the hydrogen bond predicted by theory, but experimentally not observed in the crystal state. The other large difference, of about 4°, is obtained for C1–C7–C8 and can be taken as the consequence of the free rotation. It is evident that structure obtained at the B3LYP/6-311++G(d,p) level describes the experimental values well.

3.3. NMR analysis

The experimental ^{1}H and ^{13}C NMR spectra are obtained for 3-metoxytyramine hydrochloride in DMSO as solvent. For the estimation of the chemical shifts the GIAO method is used, as it is proven to give good results for the similar chemical compounds [20,41]. The structure of **1-l** and **4-l** are used for the prediction of the NMR spectrum in order to verify the presence of both in solution. The chemical shifts are calculated relative to TMS. The chemical shifts obtained in this way are systematically overestimated because of which their values are scaled. For the comparison of the experimental and theoretical shifts the least square method is used. The scaling factors were determined based on this method and their values for ^{13}C and ^{1}H are 0.949 and 0.932, respectively. The chemical shifts are shown in Tables 2 and 3. The experimentally determined ^{1}H and ^{13}C NMR spectra are given in Supplementary material (Fig. S2 and S3).

The agreement between the experimentally and theoretically obtained data is very good, with the high correlation coefficients of 0.993 and 0.998 for ^{13}C and 0.996 for ^{1}H NMR. The better agreement for carbon atoms is usual for this type of compounds, but it should be beard in mind that in polar solvents the energy difference between the different conformers are quite low, thus allowing the presence of different conformers [41]. This is a consequence of rotation around the dihedral angles and weak interactions that are responsible for the partial stabilization of the specific conformers, because of which there are some notable differences between the experimental and theoretical results, especially for C7 and C8 which are influenced by the rotation around the dihedral angles. For the carbon atoms of the aromatic moiety the chemical shifts are reproduced very well. The agreement of data for hydrogen nuclei is also very good, but with differences in chemical shifts that are more prominent.

3.4. Vibrational spectral analysis

For the theoretical investigation **1-l** structure of 3-MT, obtained from the starting structure with crystallographic data, is used. To the best of our knowledge the experimentally obtained and assigned spectra of this important metabolite are not present in literature. It is important to mention that not the most stable conformation is used for this analysis, because it is assumed that in the solid state or solution this is not the dominant conformation. In the solid state the weak intramolecular interactions are probably overcome by the hydrogen bonds between N–H and other electronegative atoms. The total of 72 normal modes was obtained from the calculation. 3-MT is a low symmetry molecule and the most of the modes are present in both spectra, although the relative intensities are different. The scaling factor both for IR and Raman spectra of 0.980 was determined by the least square method, on the basis of the experimental IR data. The scaled values are shown in Table 4 along with the experimental wavenumbers, bands' assignments in the mid-IR region and the corresponding PED values.

Table 2
Experimental and calculated chemical shifts in ^{13}C NMR spectra for **1-l** and **4-l** structure of 3-MT (at B3LYP/6-311++G(d,p) level of theory).

Atom	Experimental chemical shift	Scaled chemical shift	
		1-l	**4-l**
C7	35	41	37
C8	43	56	49
C9	58	61	57
C2	117	111	113
C1	119	113	115
C5	125	123	125
C6	132	130	134
C3	148	152	150
C4	150	153	151
R		0.993	0.998

The scaled wavenumber values are used for further discussion. The vibrational mode peaks were assigned based on the best-fit comparison and VEDA program [27].

The data from Table 4 verify the linear correlation between the experimental and theoretical wavenumbers. The quality of this dependence was evaluated by the value of the correlation coefficient. The value of this descriptor between the experimental and theoretical wavenumbers are higher than 0.99, for both IR and Raman spectra. The comparative experimental and theoretical spectra are given in Fig. 2, and it is evident that wavenumbers are well reproduced, with the calculated intensities depending on the prominence of the specific transitions. Because the gas phase geometry was used for the comparison, a certain degree of discrepancy is expected. This is especially true for the normal modes influenced by the hydrogen bond, which is an important parameter in the solid state. This is proven when the less polar groups are compared to the polar groups (N–H and O–H), showing lower inconsistency. In the following text the most prominent bands are discussed.

The distinct broad band in the IR spectrum of 3-MT, which appears in the high frequency region (4000–2000 cm^{-1}) is assigned to the N–H stretching vibrations of the aliphatic chain (Table 4). The broadness of this mode is possibly due to the formation of the hydrogen bond within the solid phase sample, because of the presence of very polar group within the molecule. The high frequency region is also characteristic to the C–H stretching modes belonging to both, the aromatic ring as well as the aliphatic chain. The vibrational contributions to the normal stretching modes (PED values) (Table 4) in the 3440-2940 cm^{-1} region are also assigned solely to the NH and CH stretching modes themselves (98–100%) while the rest of the modes are presented as the combination of the various contributions.

Table 3
Experimental and calculated chemical shifts in ^{1}H NMR spectra for ***1-l*** and ***4-l*** structure of 3-MT (at B3LYP/6-311++G(d,p) level of theory).

Atom	Experimental chemical shift	Scaled chemical shift	
		1-l	**4-l**
H7A	2.95	3.15	2.75
H7B	2.95	3.21	3.15
H8A	3.27	3.71	3.30
H8B	3.27	3.74	3.49
H9A	3.89	4.23	3.85
H9B	3.89	4.23	3.85
H9C	3.89	4.48	4.20
H6	6.82	7.02	6.80
H2	6.99	7.03	6.90
H5	7.03	7.03	6.90
R		0.996	0.996

Table 4
Experimental and calculated positions of the bands in IR and Raman spectra of 3-MT, assignments, intensities and PED analysis of the normal modes.

Experimental			B3LYP/6-311++G(d,p)				
Mode assignment	ν_{ir} exp [cm^{-1}]	ν_{raman} exp [cm^{-1}]	ν_{scaled} [cm^{-1}]	IR intensity	Raman intensity	Raman activity	PED (%)
NH stretching (b)	3440 m		3415	0.36	69.7	1099.2	$\nu_{NH}(100)$
CH stretching (a)	3147 m	3142 vw	3138	0.00	144.7	2673.3	$\nu_{CH}(97)$
CH stretching (a)		3088 vw	3096	0.04	73.1	1383.6	$\nu_{CH}(97)$
CH stretching (b)		3068 m	3088	0.00	20.1	382.2	$\nu_{CH}(98)$
CH stretching (b)		3032 m	3029	0.01	53.3	1050.3	$\nu_{CH}(99)$
CH stretching (a)	3027 s		3022	0.11	45.4	897.1	$\nu_{CH}(99)$
CH stretching (b)		3008 m	2995	0.04	61.9	1243.4	$\nu_{CH}(97)$
CH stretching (a)		2947 vs	2957	0.15	153.9	3162.1	$\nu_{CH}(98)$
CH stretching (b)		2936 s	2954	0.14	166.6	3429.8	$\nu_{CH}(98)$
HNC bending	1623 vw		1634	0.14	7.7	395.9	$\delta_{HNC}(96)$
HNH bending (b)							
CC stretching (a)	1603 m	1616 m	1612	0.12	45.0	2366.8	$\nu_{CC}(60)$
CC stretching (a)		1593 s	1599	0.16	60.5	3221.9	$\nu_{CC}(70)$
HCC bending (a)	1526 vs	1508 vw	1517	0.89	3.1	175.8	$\delta_{HCC}(32)+ \nu_{OC}(12)+ \nu_{OC}(11)+ \nu_{CC}(22)$
CCC bending (a)							
HCH bending (b)	1506 w		1474	0.27	1.0	60.9	$\delta_{HCH}(80)$
HCC bending (b)							
HCN bending (b)							
HNC bending (b)							
HNH bending (b)							
HNC bending (b)							
HCH bending (a)	1471 w		1471	0.63	1.7	98.6	$\delta_{HCH}(78)$
HNC bending (b)							
HNH bending (b)							
HCH bending (a)	1467 vw		1465	0.05	12.2	729.8	$\delta_{HCH}(79)+ \delta_{HCH}(15)$
HCH bending (a)	1458 w		1457	0.04	3.1	185.9	$\delta_{HCH}(62)+ \nu_{CC}(10)$
HCH bending (b)		1445 s	1455	0.00	13.5	813.6	$\delta_{HCH}(90)$
CC stretching (a)	1433 w		1433	0.09	3.7	230.1	$\nu_{CC}(42)+ \delta_{HCC}(18)$
OC stretching (a)							
CC stretching (a)	1385 w		1381	0.17	18.0	1166.4	$\nu_{CC}(51)$
OC stretching (a)							
HCC bending (b)	1369 m	1371 m	1370	0.03	1.0	65.4	$\delta_{HCC}(84)$
HCH bending (b)							
HCN bending (b)							
HCN bending (b)	1326 w	1327 m	1315	0.00	4.6	320.2	$\delta H_{CN}(66)$
HCC bending (b)							
HNC bending (b)							
HOC bending (a)							
HCC bending (b)	1304 vw		1306	0.09	17.4	1214.5	δHCC(71)
HNC bending (b)							
CCN bending (b)							
HCC bending (b)		1303 w	1303	0.07	1.5	106.7	$\delta_{HCC}(62)$
HCN bending (b)							
HOC bending (a)							
HNC bending (a)							
OC stretching (b)	1279 s	1279 m	1281	1.00	22.4	1603.2	$\nu_{OC}(58)+ \delta_{HCC}(22)$
CC stretching (b)							
OC stretching (a)	1249 s		1246	0.40	1.7	127.8	$\nu_{CC}(43)$
CC stretching (a)							
HOC bending (a)	1210 m	1206 vw	1201	0.35	9.8	758.7	$\delta_{HOC}(72)$
HCC bending (a)							
CC stretching (a)	1160 vs	1150 vw	1153	0.16	4.1	338.0	$\delta_{HCC}(22) + \nu_{CC}(42)$
OC stretching (a)							
HCC bending (a)	1127 s	1131 vw	1124	0.14	0.6	53.1	$\delta_{HCH}(50)+ \nu_{CC}(10)+ \nu_{CC}(17)$
HOC bending (a)							
CC stretching (b)	1085 vw	1083 vw	1097	0.07	2.3	198.6	$\nu_{CC}(31)+ \delta_{HNC}(36)$
HCC bending (b)		1035 m	1058	0.02	1.1	100.6	$\delta_{HCC}(69)$
HNC bending (b)							
OC stretching (a)	1032 s	1025 m	1030	0.24	3.5	326.0	$\nu_{CC}(60)+ \delta_{CCC}(12)$
CC stretching (a)	957 w	957 w	934	0.09	6.5	695.7	$\nu_{CC}(44)+ \delta_{HNC}(11)$
NC stretching (b)							
OC stretching (a)							
HCCC torsion (a)	936 vw	934 w	925	0.01	0.4	38.8	$\tau_{HCCC}(94)$
NC stretching (b)	919 w	921 w	906	0.01	2.3	249.9	$\nu_{NC}(11)$
HNC bending (b)	868 w		884	0.03	1.8	202.7	$\delta_{HCH}(69)$
HCN bending (b)							
HCC bending (b)							
CCOC torsion (a)	816 s	821 vw	816	0.07	21.7	2711.7	$\tau_{HCCC}(37)+ \nu_{NC}(14)$
OC stretching (a)	799 m	803 vs	800	0.03	30.6	3912.7	$\nu_{CC}(59)$
CC stretching (a)							
HCC bending (b)	772 w		756	0.02	0.0	4.6	$\delta_{CCC}(84)$
HCN bending (b)							
HNC bending (b)							

Table 4 (*continued*)

Experimental			B3LYP/6-311++G(d,p)				
Mode assignment	ν_{ir} exp [cm^{-1}]	ν_{raman} exp [cm^{-1}]	ν_{scaled} [cm^{-1}]	IR intensity	Raman intensity	Raman activity	PED (%)
CCC bending (b) HCC bending (a) HNC bending (b)	739 vw	739 s	727	0.02	5.5	788.9	$\gamma_{OCCC}(12) + \delta_{CCC}(29) + \nu_{NC}(10)$
OCCC torsion out (a) HCCC torsion (a) CCCC torsion (a) HCCC torsion (a)	724 vw	725 w	715	0.00	2.0	292.4	$\gamma_{OCCC}(76)$
CCC bending (a) CCO bending (a)	627 w	630 w	617	0.05	1.7	291.9	$\delta_{CCC}(10) + \tau_{CCCC}(66)$
CCCC torsion (b) HCCC torsion (a) CCCO torsion (a) OCCC torsion (a)	571 w	571 m	557	0.04	3.3	631.7	$\tau_{CCCC}(12) + \delta_{CCC}(30)$
HOCC torsion (a)	460 w	454 vs	459	0.31	0.8	199.0	$\tau_{HOCC}(93)$
HOCC torsion (a) CCOC torsion (a) CCCO torsion (a) CCCC torsion (a) HCCC torsion (a)	457 w		448	0.13	0.1	23.7	$\tau_{CCCC}(83)$

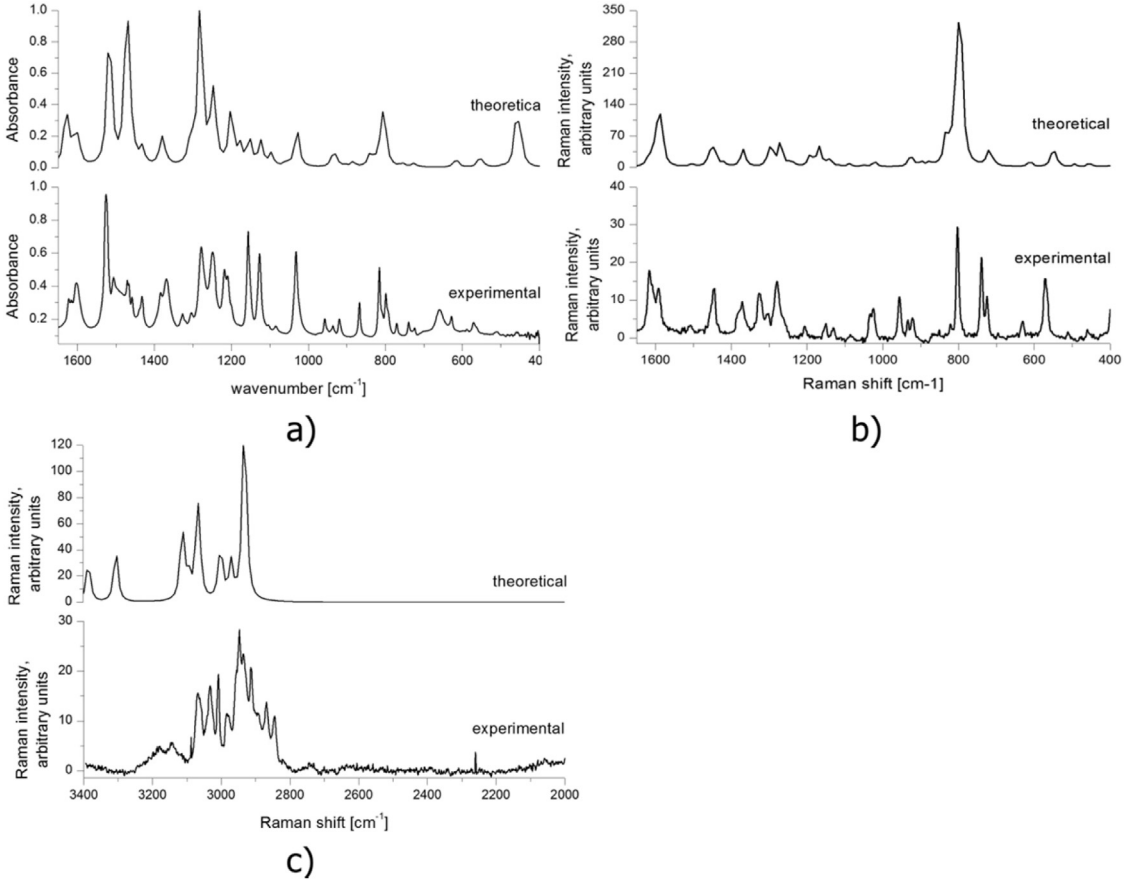

Fig. 2. Comparison between experimental and theoretical spectra of 3-MT: a) IR, 1650-400 cm^{-1}, b) Raman, 1650-400 cm^{-1} and c) Raman, 3400-2000 cm^{-1}.

The mid frequency (1700–1000 cm^{-1}) regions of the IR and normal Raman spectra (R) of 3-MT are characterized by some prominent bands. The medium to strong and very strong intensity bands at 1603 (IR), 1279 (IR), 1249 (IR), 1160 (IR), 1032 (IR), 1616 (R), 1593 (R), 1279 (R) and 1025 cm^{-1} (R) are assigned to the different, CC and CO, stretching vibrations of aromatic ring as well as of aliphatic chain. The strong to medium bands assigned to the different bending modes (HCC, CCC, HCH, HCN and HOC) of all the

structural units of 3-MT (the aromatic ring and aliphatic chain) are positioned at 1526 (IR), 1369 (IR), 1326 (IR), 1210 (IR), 1127 (IR), 1032(IR), and 1445 (R), 1371 (R), 1327 (R), 1035 (R), and 1025 (R) cm^{-1}. The mid frequency (1700–1000 cm^{-1}) regions of IR and normal Raman spectra are also characteristic to the weak intensity bands assigned as well to the different (CC and CO) stretching (1433 (IR), 1385 (IR), 1085 (IR),1150 (R) and 1083 (R) cm^{-1}) and bending modes (HCC, CCC, HCH, HCN and HOC) (1623 (IR), 1506 (IR), 1471 (IR), 1458 (IR), 1304 (IR), 1508 (R), 1303 (R), 1206 (R) and 1131(R) cm^{-1}).

In the low frequency IR and Raman regions, below 1000 cm^{-1}, the strong to medium bands, observed at 1032 (IR), 799 (IR), 1025 (R), and 803 (R) cm^{-1}, are assigned to OC, CC and NC stretching modes of the aromatic ring and aliphatic chain. The same stretching modes of low intensity are observed at 957 (IR), 919 (IR), 957 (IR) and 921 (R) cm^{-1}. The low intensity bands positioned at 868 (IR), 772 (IR), 739 (IR), 327 (IR), 725 (R) and 630 (R) cm^{-1} are assigned to CCC, CCO, HCC and HCN bending modes.

Mostly low intensity torsion modes of the benzene ring, positioned at 816 (IR), 724 (IR), 571 (IR), 460 (IR), 457 (IR), 821(IR), 725 (IR), 571(IR) and 454 (R) cm^{-1} are assigned to the different combinations of CCCC, HCCC, CCCO, HOCC and CCOC vibrations.

As it was mentioned earlier, 3-MT shows the great structural resemblance to the parent molecule dopamine and its other metabolites, for example homovanilic acid and DOPAC. The common structural parameters include the aromatic ring and aliphatic chain, just with different side groups in case of homovanillic acid and DOPAC. This structural similarity gives the possibility of a good comparison of their vibrational spectra. In the high frequency region, the OH vibration in dopamine [42] was not observed at the room temperature, but it is present in the isolated molecule of DOPAC at 15 K [19]. The rest of the characteristic vibrations in this region include NH and CH stretching modes positioned at the similar wavenumbers. In dopamine spectrum one of the most intense bands, positioned at 1512 cm^{-1}, is assigned to the CC stretching mode, while in 3-MT this band is at 1526 cm^{-1}. Other intense bands are assigned to the CO stretching mode, positioned at 1270 cm^{-3} in dopamine and 1160 cm^{-3} in 3-MT, and the mixed HCC, HOC bending and CC stretching modes, positioned at 1092/1160 (dopamine/3-MT) and 1113 cm^{-1} (DOPAC). The rest of the modes are present in the same region of the spectra, although some differences are present due to the presence of the second OH group (in dopamine and DOPAC) or the carboxyl group (in DOPAC and homovanillic acid).

3.5. UV-VIS spectra

The experimental spectrum of the water solution of 3-MT hydrochloride shows two wide peaks at 278 and 223 nm (Supplementary material, Fig. S5). The peak at 223 nm is more intense. The theoretical investigation of the electronic transition is performed on **1-l** and **4-l** structures, optimized in the aqueous phase, in order to encounter for the possible preferences of one conformer. Table 5 lists the experimental and theoretical wavelengths of the maxima as well as the theoretical composition and oscillatory strengths of the transitions. The first transition is assigned to HOMO→LUMO transition with the percentage of 78. The difference between the experimental and theoretical wavelengths for the first band, assigned to HOMO→LUMO transition, is around 20 nm. As evident from Table 5 the theoretical transition wavelengths for the second band are, for both species, well reproduced, within 5 nm. The second band, assigned to HOMO→LUMO+2 transition, is also characterized with the lower oscillatory strength for **4-l** specie. The relative heights of the maxima are better reproduced for **1-l** and for the second peak having the larger oscillatory strength.

Table 5
Theoretical transitions of protonated 3-methoxytyramine, for **1-l** conformer and **4-l** in parenthesis and italics.

Wavelengths		Theoretical composition for transition	
Experimental	Theoretical	Transition	Oscillatory str.
278	254	HOMO→LUMO (78%)	0.0735
	(257)	*(HOMO→LUMO (78%))*	*(0.0893)*
223	228	HOMO→LUMO+2 (83%)	0.1089
	(228)	*(HOMO→LUMO + 2 (60%))*	*(0.0707)*

The differences in the predicted wavelengths and experimental ones are reasonable bearing in mind that the experimental spectrum is recorded for the aqueous solution with the chloride anions present while the theoretical values are calculated for the specie in the polarizable continuum. Fig. S5 gives the comparative representation of the experimental and theoretical spectra. UV–Vis spectra cannot be used to distinguish between two conformers. In order to find the possible explanation for this observation, the molecular orbitals are visualized. Three orbitals included in the most probable transitions, namely HOMO, LUMO and LUMO+2 are given in Fig. 3 for **1-l** conformer only. The electronic density is equally distributed in **4-l**. From the introspection of the molecular orbitals, it can be concluded that the orbitals are localized on the aromatic moiety and are not influenced by the rotation of the aliphatic chain. The relatively high oscillatory strengths are due to the proximity and similarity of the orbitals included in transitions. The electronic spectra show the distinct features of the aromatic ring containing molecules with two wide bands in the near UV part of the spectrum, which proves that the aliphatic group is not influencing the lowest observable transitions. In solution, due to the specific interactions of solvent molecules, which are not included in the used theoretical model, there might be further stabilization resulting in bathochromic shift. Preferably there are interactions with the oxygen atoms of the present groups, which additionally stabilize the molecule.

3.6. NBO analysis

NBO analysis proves very useful when the stabilization interactions are concerned. The second order perturbation theory results are compared for structures in position **1**, **3** and **4** and the possible interactions of alkyl side with the aromatic ring are revealed. The most important interactions, with the stabilization energy higher than 5 kJ/mol, are listed in Table S6.

The strongest interactions present in molecule are the intermolecular hyperconjugative and resonance interactions occurring through the overlap of π(C–C) → π^*(C–C) bond orbitals. Those interactions, that are of the order of 14–74 kJ/mol, result in the weakening of the respective bonds. The rotation about the dihedral angle α does not have the influence on these interactions. Another very strong interaction is between the lone pair of oxygen atoms and the antibonding orbitals of the aromatic ring, especially those that are close to their respective positions. The strongest interactions, both with the stabilization energy between 26 and 128 kJ/mol, are established between the oxygen atom in position 1 and π^*(C4–C5) and oxygen atom in position 2 with π^*(C2–C3). Interactions of medium strength are between σO1-H σ^*C4–C5 which encounter for 20 kJ/mol. The weak hydrogen bond that is formed between O1–H···O2 additionally stabilizes the structures with energy of 5.50 kJ/mol. These interactions remain constant during the rotation.

For the conformers in position **1** the alkyl chain is very distant for any possible interactions of N–H with the aromatic ring. For the

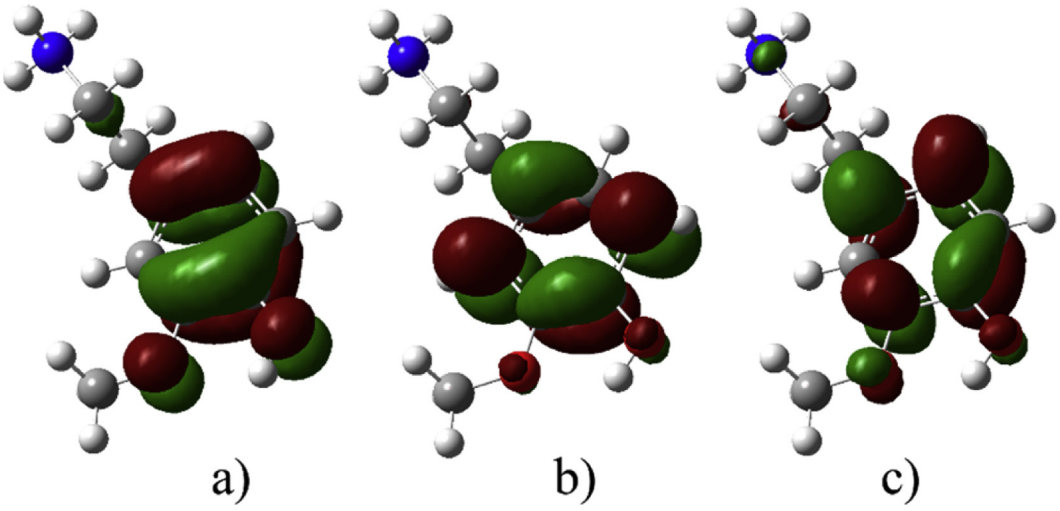

Fig. 3. Molecular orbitals of 3-MT included in electronic transitions a) HOMO, b) LUMO, and c) LUMO+2.

protonated structure **3-l** there is a donor-acceptor interaction between π(C1–C6) and σ*(N1–H) that stabilizes this structure for 9.08 kJ/mol. For **4-l** this interaction encounters for 16.74 kJ/mol of the stabilization energy, and proves that the structure **4-l** is more stabilized than the former. This data, along with the elongation of one of the N–H bonds, proves that these interactions are crucial for higher stability of the conformers 3 and 4 when compared to **1-l**. Similar situation is observed for dopamine [36].

3.7. QTAIM analysis

QTAIM analysis is performed for the additional evidence of the stabilization interactions within molecules that prove the stability of the conformers that are not experimentally observed in the crystal structure but might be present in the gaseous phase. This analysis is based on the electron density and its properties in the bond critical points and ring critical points. There are two types of the interactions: the shared interactions (covalent bonds) that are characterized by the electron density of the order of 0.1 eA and the large negative Laplacian. The second type of interactions are the closed shell interactions that include the ionic bonds, the hydrogen bonds and the van der Waals interactions, with the electron density in the range between 0.001 and 0.04 eA and the small but positive Laplacian. In this analysis only the bonds that are influenced by the rotation are present. The ring critical points of the aromatic ring are also given for the comparison between the conformers. The most important interactions are given in Table 6. The topological properties of the selected bond critical points in different conformers of 3-MT are listed in Table S7.

It is observed that all of the most stable conformers have the intramolecular hydrogen bond between hydroxyl and methoxy group (closed shell interaction). The electronic density of the bonds is not influenced by the rotation as well. In the protonated structures the change in the electronic densities for C8–N1 is about 0.06eA, thus making this bond weaker. This change is lower for the conformation where interactions of N–H with carbon atoms of the aromatic ring are present. This trend is the same for the other bonds of the aliphatic chain. For the protonated structure in positions 3 and 4 there is an intermolecular interaction between N–H and carbon atoms of the aromatic ring, thus forming the weak hydrogen bonds (carbon atoms in these positions have the negative charges). This analysis supports the NBO analysis in terms of the interactions formed during the rotation and stabilization of the molecule. These weak interactions lead to the higher stability of these conformers. The density in the ring critical points is very weakly influenced by

Table 6
Specific interactions governing stability of 3-MT conformers from QTAIM analysis.

Interactions		QTAIM		
		1-l	**3-l**	**4-l**
π(C2–C3)	σ*(N1–H10)	–	0.0164 0.0589	–
π(C1–C6)	σ*(N1–H10)	–	–	0.0169 0.0506
LP2(O2)	σ*(O1–H1)	0.0195 0.0897	0.0194 0.0898	0.0196 0.0901

Table 7
Estimated free energy of binding (E_b) and inhibition constant (K_i).

Ligand	E_b (kcal/mol)	K_i (μM)	Amino acid	Atom distance
1-l-d	−5.27	136.37	D:GLU138	2.807
			D:ASP140	1.746
			D:GLU147	2.953
			D:GLU81	2.487
			D:ASP140	2.691
			D:GLN150	2.762
3-l-d	−5.37	115.62	A:SER74	1.766
			A:GLU138	2.814
			A:ASP140	2.166
			A:ASN61	2.743
			A:GLU138	2.427
			A:GLU81	2.396
4-l-d	−5.50	93.18	B:ASP140	2.455
			B:GLU138	2.109
			B:GLN139	2.562
			B:GLU81	2.409
1-l	−5.24	144.01	A:GLU138	2.531
			A A:GLU138	2.765
			A:ASP140	2.145
			A:SER74	2.173
3-l	−5.75	60.95	B:GLU147	2.152
			B:GLU138	2.791
			B:ASP140	2.306
			B:ASP140	2.191
			B:GLU81	3.069
4-l	−5.60	78.62	B:GLU147	2.333
			B:GLU138	2.640
			B:ASP140	2.435
			B:ASP140	2.061

the rotation, except in cases of the stable conformation of the protonated 3-MT, because of the interactions between N–H and carbon atoms of the aromatic ring.

The topological parameters for the structures optimized in water are given in Supplementary material, Table S8. There are no bond critical points between N–H and carbon atoms of the aromatic ring as in the gaseous phase probably due to a stronger influence of the polarizable continuum. The changes in parameters with dilution are decrease in the electron density and increase in Laplacian, thus proving that bonds are becoming weaker when 3-MT is diluted. Because there are no stabilization interactions present, the change in energy and Gibbs free energy between the conformers is much lower than in the gaseous phase thus allowing the simultaneous presence of the several conformers, as discussed in NMR analysis.

3.8. Molecular docking analysis

As it was shown in previous sections there is a significant discrepancy between the crystal structure and the most stable conformations in gaseous and aqueous phase, due to the specific interactions as explained by NBO and QTAIM. Because 3-MT is highly important molecule in biological systems and the major extracellular metabolite of neurotransmitter dopamine, the molecular docking is performed in order to investigate the most stable conformations of the protonated and deprotonated 3-MT. Also, this technique helps in obtaining the protein-ligand binding energy and identifying the potential ligand binding sites. This investigation includes both the protonated and deprotonated forms of the most stable conformers (the deprotonated are marked with –**d**). Determination of 3-MT conformation that is crucial for the binding to the certain protein molecule is done by selecting the one that shows the lowest binding energy (the best pose). The position and orientation of 3-MT ligands in protein receptor, and the interaction with the amino acids that bound to the ligand, are analyzed and visualized with Discovery Studio 4.0 and AutoDockTools.

The estimated free energy of binding and the most favorable binding positions for each of the investigated conformers is given in

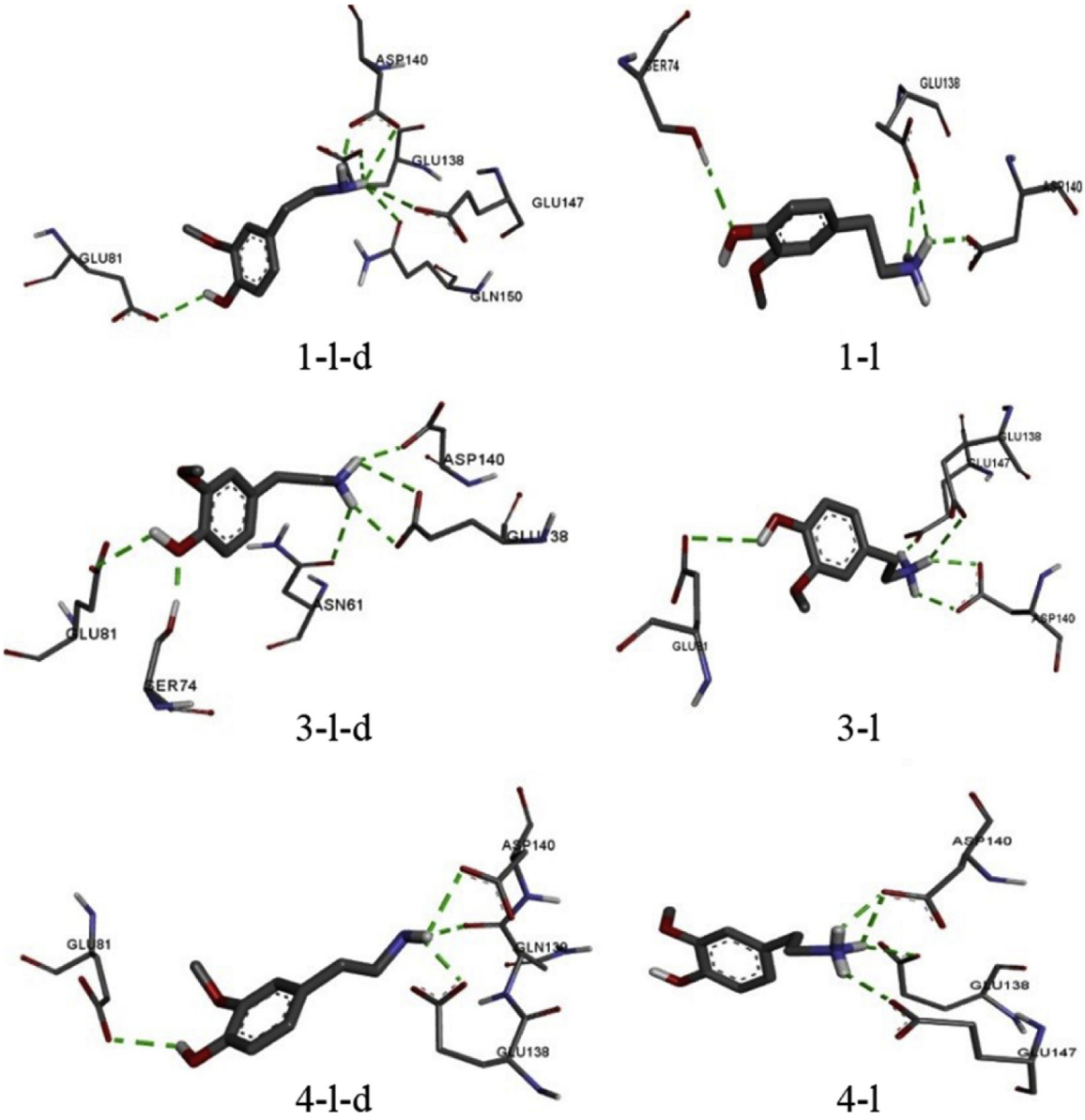

Fig. 4. Possible interactions between selected 3-MT ligands and protein.

Table 7. The lower value of Ki indicates the better inhibition. Fig. 4 gives an overview of the selected positions of 3-MT and protein.

The obtained results from Table 7 show that the protonated forms of 3-MT, **3-l** and **4-l**, are more interactive and are binding more strongly than the deprotonated forms. It is important to take a careful look at the conformation of the investigated molecule after the optimization in protein is done. None of the final conformations have the aliphatic chain above the aromatic ring, thus proving that interactions between these two parts of the molecule are very weak and easily broken if the other interactions are possible with the surrounding molecules. It is important to notice that the most active deprotonated conformation, **4-l-d**, resembles the protonated structure proposed by Okabe et al. [35], which is described as very reactive one and similar to the biologically active conformation of dopamine. For the protonated form the final conformations of **3-l** and **4-l** are almost identical to **1-l** obtained by DFT calculation, thus proving that this structure is more realistic than the former ones. Analyzing the position of the active amino acids (Table 7 and Fig. 4), it can be concluded that Glutamic acid in position 147, in the primary structure of any chain, and Aspartic acid in position 140 have the predominant role as the active sites of CRP for the inhibition action, regardless of the ligand used.

4. Conclusion

In this contribution, 3-metoxytyramine, an important metabolite of dopamine has been characterized by several spectroscopic techniques (UV-VIS, IR, Raman and NMR). The density functional calculations, performed on the suggested crystallographic structure with the conformational search, show that there are 12 stable conformations in total. All of these are optimized on B3LYP/6-311++G(d,p) level and compared. The most stable conformer resembles that of dopamine, determined previously. The detailed analysis of these interactions is given in paper. The difference between two of the most stable structures in vacuum is 18 kJ/mol showing that the rotation can occur. When structures are optimized in water, the most of weak interactions are lost. Due to the formation of the weak interactions between N–H and π system, as proven by the NBO and QTAIM analysis, the most stable conformers in vacuum are different from the experimentally determined crystallographic structure. The structure determined by the conformation search is compared to the crystallographic structure of 3-methoxytyramine perchlorate, and with an average difference of 0.02–0.04 Å and 1-2° for angles. The ^{1}H and ^{13}C NMR spectra are compared and the obtained correlation coefficients are higher than 0.99 for both of the available spectra. The discrepancy between the experimental and theoretical values can be due to the fact that the free rotation is possible and thus the resonance maxima are highly dependent upon it. The vibrational analysis gives very good agreement between the applied DFT method and experimental results, except for the high frequency region where some of the distinctive peaks are not observed. Because the calculations are performed on the isolated molecule, without the influence of the specific interactions, while the vibrational spectra were recorded for solid KBr pastille, any difference is due to this fact. The UV bands are attributed to $\pi \rightarrow \pi^*$ transitions within the aromatic ring. Because these calculations are also performed for the isolated molecule, any solvent effect manifested through the hydrogen bonding can move the peak position. The relative bands' intensities and widths are reproduced well.

Acknowledgement

The authors acknowledge financial support by the Ministry of Education, Science and Technological Development of the Republic of Serbia (Grants No. 172015 and 172040). The authors thank Prof. Jamróz MH for VEDA 4 program.

Appendix A. Supplementary data

Supplementary data related to this article can be found at http://dx.doi.org/10.1016/j.molstruc.2016.12.082.

References

[1] J.C. Fitzgerald, H. Plun-Favreau, Emerging pathways in genetic Parkinson's disease: autosomal-recessive genes in Parkinson's disease - a common pathway? FEBS J. 275 (23) (2008) 5758–5766.
[2] S.W. Kim, H.S. Ko, V.L. Dawson, T.M. Dawson, Recent advances in our understanding of Parkinson's disease, Drug Discov. Today Dis. Mech. 2 (4) (2005) 427–433.
[3] F. Karoum, S.J. Chrapusta, M.F. Egan, 3-Methoxytyramine is the major metabolite of released dopamine in the rat frontal cortex: reassessment of the effects of antipsychotics on the dynamics of dopamine release and metabolism in the frontal cortex, nucleus accumbens, and striatum by a simple T, J. Neurochem. 63 (3) (Nov. 2002) 972–979.
[4] T.D. Sotnikova, J.-M. Beaulieu, S. Espinoza, B. Masri, X. Zhang, A. Salahpour, L.S. Barak, M.G. Caron, R.R. Gainetdinov, The dopamine metabolite 3-methoxytyramine is a neuromodulator, PLoS One 5 (10) (2010) e13452.
[5] B.H.C. Westerink, S.J. Spaan, On the significance of endogenous 3-methoxytyramine for the effects of centrally acting drugs on dopamine release in the rat brain, J. Neurochem. 38 (3) (Mar. 1982) 680–686.
[6] J.W.M. Lenders, K. Pacak, M.M. Walther, W.M. Linehan, M. Mannelli, P. Friberg, H.R. Keiser, D.S. Goldstein, G. Eisenhofer, Biochemical diagnosis of pheochromocytoma - which test is the best, JAMA 287 (11) (Mar. 2002) 356–368.
[7] G. Eisenhofer, D.S. Goldstein, R. Stull, Simultaneous liquid-chromatographic determination of 3,4-dihydroxyphenylglycol, catecholamines, and 3,4-dihydroxyphenylalanine in plasma, and their responses to inhibition of monoamine oxidase, Clin. Chem. 32 (11) (1986) 3030–3033.
[8] G. Eisenhofer, J.W.M. Lenders, K. Pacak, Biochemical diagnosis of pheochromocytoma, in: Pheochromocytoma, vol. 31, KARGER, Basel, 2003, pp. 76–106.
[9] M. Peitzsch, D. Pelzel, S. Glöckner, A. Prejbisz, M. Fassnacht, F. Beuschlein, A. Januszewicz, G. Siegert, G. Eisenhofer, Simultaneous liquid chromatography tandem mass spectrometric determination of urinary free metanephrines and catecholamines, with comparisons of free and deconjugated metabolites, Clin. Chim. Acta 418 (2013) 50–58.
[10] J.W. Lenders, G. Eisenhofer, M. Mannelli, K. Pacak, Phaeochromocytoma, Lancet 366 (9486) (2005) 665–675.
[11] G. Eisenhofer, J.W.M. Lenders, G. Siegert, S.R. Bornstein, P. Friberg, D. Milosevic, M. Mannelli, W.M. Linehan, K. Adams, H.J. Timmers, K. Pacak, Plasma methoxytyramine: a novel biomarker of metastatic pheochromocytoma and paraganglioma in relation to established risk factors of tumour size, location and SDHB mutation status, Eur. J. Cancer 48 (11) (2012) 1739–1749.
[12] G. Eisenhofer, M. Peitzsch, Laboratory evaluation of pheochromocytoma and paraganglioma, Clin. Chem. 60 (12) (Dec. 2014) 1486–1499.
[13] J.W.M. Lenders, Q.-Y. Duh, G. Eisenhofer, A.-P. Gimenez-Roqueplo, S.K.G. Grebe, M.H. Murad, M. Naruse, K. Pacak, W.F. Young, Pheochromocytoma and paraganglioma: an endocrine society clinical practice guideline, J. Clin. Endocrinol. Metab. 99 (6) (Jun. 2014) 1915–1942.
[14] F. Patin, L. Crinière, T. Francia, S. Kassem, P. Pierre, C. Bruno, C. Vayne, P. Vourc'h, I. Benz-de Bretagne, C.R. Andres, H. Blasco, Low Specificity of Urinary 3-methoxytyramine in Screening of Dopamine-secreting Pheochromocytomas and Paragangliomas, 2016.
[15] B.H.C. Westernik, J. Korf, Rapid concurrent automated fluorimetric assay of noradrenaline, dopamine, 3,4-dihidroxyphenylacetic acid, homovanillic acid and 3-methoxytyramine in milligram amounts of nervous tissue after isolation on Sephadex G10, J. Neurochem. 29 (4) (Oct. 1977) 697–706.
[16] R.E. Shoup, P.T. Kissinger, Determination of urinary normetanephrine, metanephrine, and 3-methoxytyramine by liquid chromatography, with amperometric detection, Clin. Chem. 23 (7) (Jul. 1977) 1268–1274.
[17] F. Gosetti, E. Mazzucco, M.C. Gennaro, E. Marengo, Simultaneous determination of sixteen underivatized biogenic amines in human urine by HPLC-MS/MS, Anal. Bioanal. Chem. 405 (2–3) (Jan. 2013) 907–916.
[18] C.L. Galli, F. Cattabeni, T. Eros, P.F. Spano, S. Algeri, A. Di Giulio, A. Groppetti, A mass fragmentic assay of 3-metoxytyramine in rat brain, J. Neurochem. 27 (3) (Sep. 1976) 795–798.
[19] A.J. Lopes Jesus, S. Jarmelo, R. Fausto, I. Reva, Conformational preferences of 3,4-dihydroxyphenylacetic acid (DOPAC), Spectrochim. Acta. A. Mol. Biomol. Spectrosc. 140 (Apr. 2015) 54–64.
[20] M. Samsonowicz, M. Kowczyk-Sadowy, E. Regulska, W. Lewandowski, Molecular structure and spectroscopic analysis of homovanillic acid and its sodium salt – NMR, FT-IR and DFT studies, Spectrochim. Acta Part A Mol. Biomol. Spectrosc. 118 (2014) 1068–1074.
[21] R. Wysokiński, K. Hernik, R. Szostak, D. Michalska, Electronic structure and vibrational spectra of cis-diammine(orotato)platinum(II), a potential cisplatin analogue: DFT and experimental study, Chem. Phys. 333 (1) (2007) 37–48.
[22] M.J. Frisch, G.W. Trucks, H.B. Schlegel, G.E. Scuseria, M.A. Robb,

J.R. Cheeseman, G. Scalmani, V. Barone, B. Mennucci, G.A. Petersson, H. Nakatsuji, M. Caricato, X. Li, H.P. Hratchian, A.F. Izmaylov, J. Bloino, G. Zheng, J.L. Sonnenberg, M. Hada, M. Ehara, K. Toyota, R. Fukuda, J. Hasegawa, M. Ishida, T. Nakajima, Y. Honda, O. Kitao, H. Nakai, T. Vreven, J. Montgomery, J.E. Peralta, F. Ogliaro, M. Bearpark, J.J. Heyd, E. Brothers, K.N. Kudin, V.N. Staroverov, R. Kobayashi, J. Normand, K. Raghavachari, A. Rendell, J.C. Burant, S.S. Iyengar, J. Tomasi, M. Cossi, N. Rega, J.M. Millam, M. Klene, J.E. Knox, J.B. Cross, V. Bakken, C. Adamo, J. Jaramillo, R. Gomperts, R.E. Stratmann, O. Yazyev, A.J. Austin, R. Cammi, C. Pomelli, J.W. Ochterski, R.L. Martin, K. Morokuma, V.G. Zakrzewski, G.A. Voth, P. Salvador, J.J. Dannenberg, S. Dapprich, A.D. Daniels, Ö. Farkas, J.B. Foresman, J.V. Ortiz, J. Cioslowski, D.J. Fox, Gaussian 09, Gaussian, Inc, Wallingford CT, 2009.

[23] A.D. Becke, Density-functional thermochemistry. III. The role of exact exchange, J. Chem. Phys. 98 (7) (Apr. 1993) 5648.

[24] T.H. Dunning, Gaussian basis sets for use in correlated molecular calculations. I. The atoms boron through neon and hydrogen, J. Chem. Phys. 90 (2) (Jan. 1989) 1007.

[25] A.V. Marenich, C.J. Cramer, D.G. Truhlar, Universal solvation model based on solute electron density and on a continuum model of the solvent defined by the bulk dielectric constant and atomic surface tensions, J. Phys. Chem. B 113 (18) (2009) 6378–6396.

[26] Time-dependent density-functional theory for molecules and molecular solids, J. Mol. Struct. THEOCHEM 914 (1) (2009) 3–18.

[27] M.H. Jamróz, VEDA 4Warsaw, 2004.

[28] R.A. Munos, Y.N. Panchenko, G.S. Koptev, N.F. Stepanov, Program for calculating distribution of potential energy in internal coordinates, J. Appl. Spectrosc. 12 (3) (Mar. 1970) 428–429.

[29] R. Ditchfield, Self-consistent perturbation theory of diamagnetism, Mol. Phys. 27 (4) (Apr. 1974) 789–807.

[30] K. Wolinski, J.F. Hinton, P. Pulay, Efficient implementation of the gauge-independent atomic orbital method for NMR chemical shift calculations, J. Am. Chem. Soc. 112 (23) (Nov. 1990) 8251–8260.

[31] J.P. Foster, F. Weinhold, Natural hybrid orbitals, J. Am. Chem. Soc. 102 (24) (Sep. 1980) 7211–7218.

[32] R.F.W. Bader, Atoms in molecules, Acc. Chem. Res. 18 (1) (Jan. 1985) 9–15.

[33] D. Thompson, M.B. Pepys, S.P. Wood, The physiological structure of human C-reactive protein and its complex with phosphocholine, Structure 7 (2) (1999) 169–177.

[34] BIOVIA Discovery Studio 2016, Accelrys Studio Inc, San Diego, 2016.

[35] N. Okabe, S. Mori, Y. Sasaki, Structure of 3-Metoxytyramine hydrochloride, Acta Crystallogr. Sect. A1 48 (1991) 1448–1450.

[36] A. Lagutschenkov, J. Langer, G. Berden, J. Oomens, O. Dopfer, Infrared spectra of protonated neurotransmitters: dopamine, Phys. Chem. Chem. Phys. 13 (7) (Feb. 2011) 2815–2823.

[37] J.J. Urban, C.W. Cronin, R.R. Roberts, G.R. Famini, Conformational preferences of 2-phenethylamines. A computational study of substituent and solvent effects on the intramolecular amine-aryl interactions in charged and neutral 2-phenethylamines, J. Am. Chem. Soc. 119 (50) (1997) 12292–12299.

[38] P.I. Nagy, G. Alagona, C. Ghio, Theoretical studies on the conformation of protonated dopamine in the gas phase and in aqueous solution, J. Am. Chem. Soc. 121 (20) (1999) 4804–4815.

[39] P.I. Nagy, G.J. Durant, W.P. Hoss, D.A. Smith, Theoretical analyses of the tautomeric and conformational equilibria of histamine and (alphaR,betaS)-alpha,beta-Dimethylhistamine in the gas phase and in aqueous solution, J. Am. Chem. Soc. 116 (1994) 4898–4909.

[40] N. Okabe, S. Mori, Structure of 3-methoxytyramine perchlorate, Acta Crystallogr. Sect. C Cryst. Struct. Commun. 48 (9) (1992) 1698–1699.

[41] S. Marković, J. Tošović, J.M. Dimitrić Marković, Synergic application of spectroscopic and theoretical methods to the chlorogenic acid structure elucidation, Spectrochim. Acta Part A Mol. Biomol. Spectrosc. 164 (2016) 67–75.

[42] N. Misra, Vibrational dynamics and potential energy distribution of two well-known 8 (3) (2009) 433–450.